Atmospheric Moisture Decreases Midlatitude Eddy Kinetic Energy

NICHOLAS J. LUTSKO,[a] JOSÉ MARTINEZ-CLAROS,[a] AND DANIEL D. B. KOLL[b]

[a] *Scripps Institution of Oceanography, University of California at San Diego, La Jolla, California*
[b] *Laboratory for Climate and Ocean-Atmosphere Studies, Department of Atmospheric and Oceanic Sciences, Peking University, Beijing, China*

(Manuscript received 5 December 2023, in final form 11 July 2024, accepted 25 July 2024)

ABSTRACT: There is compelling evidence that atmospheric moisture may either increase or decrease midlatitude eddy kinetic energy (EKE). We reconcile these findings by using a hierarchy of idealized atmospheric models to demonstrate that moisture energizes individual eddies given fixed large-scale background winds and temperatures but makes those background conditions less favorable for eddy growth. For climates similar to the present day, the latter effect wins out, and moisture weakens midlatitude eddy activity. The model hierarchy includes a moist two-layer quasigeostrophic (QG) model and an idealized moist general circulation model (GCM). In the QG model, EKE increases when moisture is added to simulations with fixed baroclinicity, closely following a previously derived scaling. But in both models, moisture decreases EKE when environmental conditions are allowed to vary. We explain these results by examining the models' mean available potential energy (MAPE) and by calculating terms in the models' Lorenz energy cycles. In the QG model, the EKE decreases because precipitation preferentially forms on the poleward side of the jet, releasing latent heat where the model is relatively cold and decreasing the MAPE, hence the EKE. In the moist GCM, the MAPE primarily decreases because the midlatitude stability increases as the model is moistened, with reduced meridional temperature gradients playing a secondary role. Together, these results clarify moisture's role in driving the midlatitude circulation and also highlight several drawbacks of QG models for studying moist processes in midlatitudes.

SIGNIFICANCE STATEMENT: Dry models of the atmosphere have played a central role in the study of large-scale atmospheric dynamics. But we know that moisture adds much complexity, associated with phase changes, its effect on atmospheric stability, and the release of latent heat during condensation. Here, we take an important step toward incorporating moisture into our understanding of midlatitude dynamics by reconciling two diverging lines of literature, which suggest that atmospheric moisture can either increase or decrease midlatitude eddy kinetic energy. We explain these opposing results by showing that moisture not only makes individual eddies more energetic but also makes the environment in which eddies form less favorable for eddy growth. For climates similar to the present day, the latter effect wins out such that moisture decreases atmospheric eddy kinetic energy. We demonstrate this point using several different idealized atmospheric models, which allow us to gradually add complexity and to smoothly vary between moist and dry climates. These results add fundamental understanding to how moisture affects midlatitude climates, including how its effects change in warmer and moisture climates, while also highlighting some drawbacks of the idealized atmospheric models.

KEYWORDS: Atmospheric circulation; Dynamics; Eddies; Extratropical cyclones

1. Introduction

Much of our understanding of midlatitude dynamics comes from dry models of the atmosphere. Both individual weather systems and the mean state of the midlatitude atmosphere can be usefully studied while neglecting atmospheric water vapor, eliminating the complications of phase changes and associated latent heat release. Despite the advantages of this simplification, it is clear that moisture does affect midlatitude eddy activity. Idealized calculations show that latent heat release increases the linear growth rate and kinetic energy of moist baroclinic eddies (Bannon 1986; Emanuel et al. 1987; Gutowski et al. 1992; Zurita-Gotor 2005; Kirshbaum et al. 2018; Kohl and O'Gorman 2022; Brown et al. 2023), while simulations of individual events have confirmed the crucial role of latent heating in storm intensification (e.g., Reed et al. 1988; Wernli et al. 2002; Joos and Wernli 2012). Ignoring the reduced static stability in the presence of moisture causes models to underestimate the eddy kinetic energy (EKE) of the storm tracks (Chang 2006; O'Gorman 2011), and Chang et al. (2002) further showed that moisture contributes positively to the budget of eddy available potential energy (EAPE) in reanalysis data [though the baroclinic life cycle calculations of Kirshbaum et al. (2018) suggest that this effect is sensitive to the phasing of eddy fields and weakens in warmer climates]. Brown et al. (2023) recently developed an alternative way of describing moisture's contribution to the EAPE budget by defining a "moist energy" that is converted into EAPE by precipitation in the warm sectors of extratropical cyclones. Long before these results, Lorenz (1979) found that the mean available potential energy (MAPE) of the atmosphere is always greater when the potential release of

Denotes content that is immediately available upon publication as open access.

Corresponding author: Nicholas Lutsko, nlutsko@ucsd.edu

DOI: 10.1175/JAS-D-23-0226.1

latent heat due to condensation of water vapor is taken into account, though the precise relationship between moist MAPE and EKE is still unclear.

On the other hand, studies of both idealized atmospheric general circulation models (GCMs; see O'Gorman and Schneider 2008b; Schneider et al. 2010) and comprehensive climate models and reanalysis data (O'Gorman 2010; Gertler and O'Gorman 2019) have found that midlatitude EKE scales linearly with the dry MAPE, which maximizes in climates similar to that of Earth's present day and decreases in warmer, and moister, climates (see also Manabe and Wetherald 1975, 1980). In more direct tests, simulations with idealized GCMs have found that increasing atmospheric moisture while keeping temperature fixed decreases midlatitude EKE (Frierson et al. 2006; Bembenek et al. 2020; Lutsko and Hell 2021). Bembenek et al. (2020) analyzed the energy budget of their two-layer moist shallow water simulations and found that precipitation acts as an energy sink, leaving less energy that can be converted from MAPE into EAPE and in turn from EAPE into EKE.

So, there is compelling evidence that moisture may either increase or decrease midlatitude EKE. In this study, we reconcile these opposing results by drawing a distinction between moisture's effect on individual eddies—which it makes more energetic—and its effect on the large-scale conditions in which eddies form—which it makes less favorable for eddy growth. In all the situations we consider, the latter effect wins out, such that including moisture increases the EKE for a given environment or a given storm but weakens EKE when environmental conditions are allowed to vary.

We demonstrate how moisture's impact on EKE depends on the large-scale environment using simulations with a hierarchy of idealized atmospheric models, systematically varying between the moist and dry limits. We begin with a moist, two-layer quasigeostrophic (QG) model. Two-layer QG models have played a fundamental role in our understanding of midlatitude dynamics and are commonly run either in homogeneous setups with fixed, uniform baroclinicity (e.g., Haidvogel and Held 1980; Panetta 1993; Pavan and Held 1996; Held and Larichev 1996) or in channel configurations, where the mean flow is relaxed to an equilibrium profile but is otherwise free to evolve (e.g., Lee and Held 1993; Zurita-Gotor et al. 2014; Zurita-Gotor 2014; Lutsko et al. 2015, 2017). Most previous work on two-layer QG models has focused on dry models, but Lapeyre and Held (2004) introduced a moist homogeneous QG model that Lutsko and Hell (2021) extended to a channel geometry (see also Bouchut et al. 2009; Laîné et al. 2011; Lambaerts et al. 2011a,b, 2012, for closely related studies of moist two-layer shallow water models). By running simulations in both setups, we show that in the same dynamical system, moisture can either increase EKE (in the homogeneous case with fixed baroclinicity) or decrease EKE (in the channel case when the baroclinicity can adjust).

The suitability of two-layer QG models for studying moist processes is still an open question, so we have also studied a moist, gray radiation GCM that has been widely used by the atmospheric dynamic community (e.g., Frierson et al. 2006, 2007; O'Gorman and Schneider 2008a,b; Schneider et al. 2010; Levine and Schneider 2015; Bischoff and Schneider 2016; Lutsko and Popp 2018; Wills and Schneider 2018; Lutsko et al. 2019). The stratification has more freedom to respond to changing thermodynamic conditions in the gray radiation GCM than in the QG model, and the GCM includes other dynamically relevant factors, such as the tropopause height, that are not represented in the two-layer QG model. Since the GCM uses a fixed profile of longwave optical depths, it can be smoothly varied between the moist and dry limits; in a model with an active water vapor feedback, the effects of atmospheric moisture would have to be separated from large global-mean warming and cooling of the model.

Midlatitude EKE decreases as moisture is added to the GCM, which we investigate by examining changes in MAPE and by considering the GCM's energy budget, also known as the Lorenz energy cycle (Lorenz 1955). As mentioned above, previous studies have found a linear relationship between MAPE and midlatitude EKE in simulations mimicking changes in atmospheric carbon dioxide (CO_2) concentrations, so we begin by analyzing how MAPE changes when moving between dry and moist climates. Next, we calculate the terms in the energy budgets of the simulations, highlighting the importance of latent heat release in driving eddy activity at midlatitudes, especially the location where latent heat release occurs. Comparing the moist GCM to the QG model reveals key drawbacks of the latter for studying moist dynamics. Most strikingly, the energy cycles of the moist GCM simulations resemble the "strong moisture" regime of the QG model, where the flow is characterized by strong low-level cyclones and weak upper-level anticyclones. Although the flow in the strong moisture regime is qualitatively different from what is observed in Earth's midlatitudes [it is more reminiscent of the "TC Worlds" seen in simulations of rotating radiative–convective equilibrium; e.g., Held and Zhao (2008), Zhou et al. (2017)], from an energetic perspective, at least, this regime seems to be a closer analog to Earth's atmosphere than QG simulations with weak, but more realistic, latent heating.

The paper is structured as follows. In sections 2 and 3, we describe and analyze the homogeneous and channel configurations of the moist QG model, respectively. Then, the moist GCM simulations are presented and analyzed in section 4. We end with conclusions in section 5, which includes discussion of the links between our results and previous work on atmospheric entropy budgets.

2. Homogeneous quasigeostrophic model

a. Model description

The homogeneous moist QG model numerically solves the system first proposed by Lapeyre and Held (2004), consisting of two constant density layers on a β plane in a doubly periodic domain, with moisture added as an active tracer in the lower layer. The zonal-mean winds vary linearly in the y direction, such that the zonal-mean potential vorticity (PV) gradient in each layer is $Q_k = \beta + (-1)^{k+1}U$, where $U_1 = -U_2 = U/2$ and $k = 1$ in the upper layer and $k = 2$ in the lower layer. Ekman friction is added to the lower layer.

The (nondimensionalized) dynamical equations in this system follow PV anomalies:

$$\frac{\partial}{\partial t}q_k(x,y,t) + J[\psi_k(x,y,t), q_k(x,y,t)] = (-1)^k\frac{\partial}{\partial x}q_k(x,y,t) - [\beta - (-1)^k]\frac{\partial}{\partial x}\psi_k(x,y,t) - \frac{1}{\tau_f}\delta_{k2}\nabla^2\psi_k(x,y,t) + (-1)^k LP(x,y,t) - \nu\nabla^4 q_k(x,y,t), \tag{1}$$

where $q_k = \nabla^2\psi_k + (-1)^k(\psi_1 - \psi_2)$ is the spatially varying PV anomaly in each layer; the ψ_k represents the streamfunctions; J is the Jacobian operator; τ_f is a frictional time scale acting only in the lower layer; ν is a hyperdiffusion coefficient; L is the nondimensionalized latent heat of vaporization; and P is the anomalous precipitation (see below).

Moisture is represented as a nondimensionalized mixing ratio and is decomposed into a domain-mean mixing ratio M and an anomalous mixing ratio m. The term M evolves as

$$\frac{\partial M(t)}{\partial t} = E - \Pi(t), \tag{2}$$

where E is a specified, constant domain-mean evaporation rate and Π is the domain-mean precipitation. The anomalous moisture evolves as

$$\frac{\partial}{\partial t}m(x,y,t) + J[\psi_2(x,y,t), m(x,y,t)] = \frac{1}{2}\frac{\partial}{\partial x}m(x,y,t) + C\frac{\partial}{\partial x}\psi_2(x,y,t) - P(x,y,t) - \nabla\cdot\mathbf{u}_2(x,y,t), \tag{3}$$

where C is a constant that relates the saturation mixing ratio m_s and the temperature $\psi_1 - \psi_2$ in a linearization of the Clausius–Clapeyron relation: $m_s \equiv C(\psi_1 - \psi_2)$. The last term on the right-hand side of Eq. (3) is a linearization of ageostrophic advection in the lower layer. We note that length scales are nondimensionalized using the Rossby deformation radius λ, time scales by the ratio of λ to the mean zonal wind shear U and m by $m_0U/(f_0\lambda)$, where m_0 is a reference lower-tropospheric mixing ratio. The reader is referred to Lapeyre and Held (2004) for a full derivation of this system.

The total precipitation at a grid point is equal to $\Pi + P$ and instantaneously resets $(1 + CL)M + m$ to the saturation mixing ratio whenever it rises above this value. The addition of moisture and precipitation complicates the numerics of the model, and we follow the approach described in the appendix of Lapeyre and Held (2004) to calculate the precipitation and $\nabla\cdot\mathbf{u}_2$ (see also Lutsko and Hell 2021).

We have run linear and nonlinear experiments with the homogeneous QG model on a grid of size $10\pi \times 10\pi$, with 256 grid points in each direction. The linear experiments allow us to estimate eddy growth rates that can be compared to previously derived scalings, while the nonlinear experiments show how EKE depends on moisture in this system. In the linear experiments, nonlinear eddy interactions are turned off and small-scale noise is added to the streamfunction and moisture fields to initiate instability. These experiments are run for 100 model time units, with averages taken over the last 50 model time units (1 time unit $\approx$ 0.57 Earth days in these simulations). The nonlinear experiments are run for 2000 model time units, with the first 1000 time units discarded as spinup.

Our default parameters are $\beta = 0.78$, $L = 0.2$, $C = 2$, and $E = 1.39$, again following Lapeyre and Held (2004). We have run linear and nonlinear experiments with L varied from 0 to 0.99, holding $C = 2$, and with C ranging from 0 to 4, holding $L = 0.2$. These can be thought of, roughly, as varying the strength of latent heating and varying the rate at which atmospheric water vapor increases with warming, respectively, though the nondimensional L and C both depend on the dimensional latent heat of vaporization. We have also varied the evaporation rate E, but for ease of presentation focus here on the experiments with varying L and C. Our control value of $E = 1.39$ is substantially higher than the realistic value of 0.4 estimated by Lapeyre and Held (2004), but the results are qualitatively similar with E set to 0.4 (not shown).

b. Linear and nonlinear simulations

In the linear simulations, the eddy growth rate σ increases monotonically with L, from roughly 0.12 for $L = 0$ to roughly 0.36 for $L = 0.99$ (Fig. 1a[1]), consistent with past work suggesting that latent heat release increases eddy growth rates. Zurita-Gotor (2005) derived a scaling for eddy growth rates in moist QG systems that predicts σ decreases with the effective stability r:

$$\sigma = \frac{-(r+1) + \sqrt{(r+1)^2 + 4r}}{2r}. \tag{4}$$

An effective stability can be defined for our system as $r = (1 - L)/(1 + CL)$ (Lapeyre and Held 2004), and the red curve in Fig. 1b shows that Eq. (4) produces an excellent match to the simulated growth rates, which increase rapidly as the effective stability decreases (note that in Fig. 1b, σ is multiplied by a constant obtained by linear least squares regression). Equation (4) works well despite being derived on an f plane, rather than a β plane, as used here. Emanuel et al. (1987) derived a different scaling for moist growth rates in a semigeostrophic system, but their scaling does not match the results here well [Fig. 1a of Zurita-Gotor (2005) provides a comparison of the two scalings]. Qualitatively, the Emanuel et al. (1987) prediction is similar: Eddy growth rates increase as the effective stability decreases.

The nonlinear simulations show that EKE also increases with L in the homogeneous QG system (Fig. 1c), and similar results are seen in the experiments with varying C (triangles in Fig. 1d). If eddy length scales are assumed to be constant, then the EKE should scale as σ^2, and we confirm in Fig. 1d that Eq. (4) provides a good fit to the simulated EKE in both the simulations with varying L and with varying C (we experimented with other integer powers of σ and confirmed that the square does give the best fit). As L is increased, the model transitions to the strong moisture regime described in the

[1] Growth rates are calculated as $\sigma = \log(|\psi_1'|_1/|\psi_1'^{-1}|_1)/\Delta t$

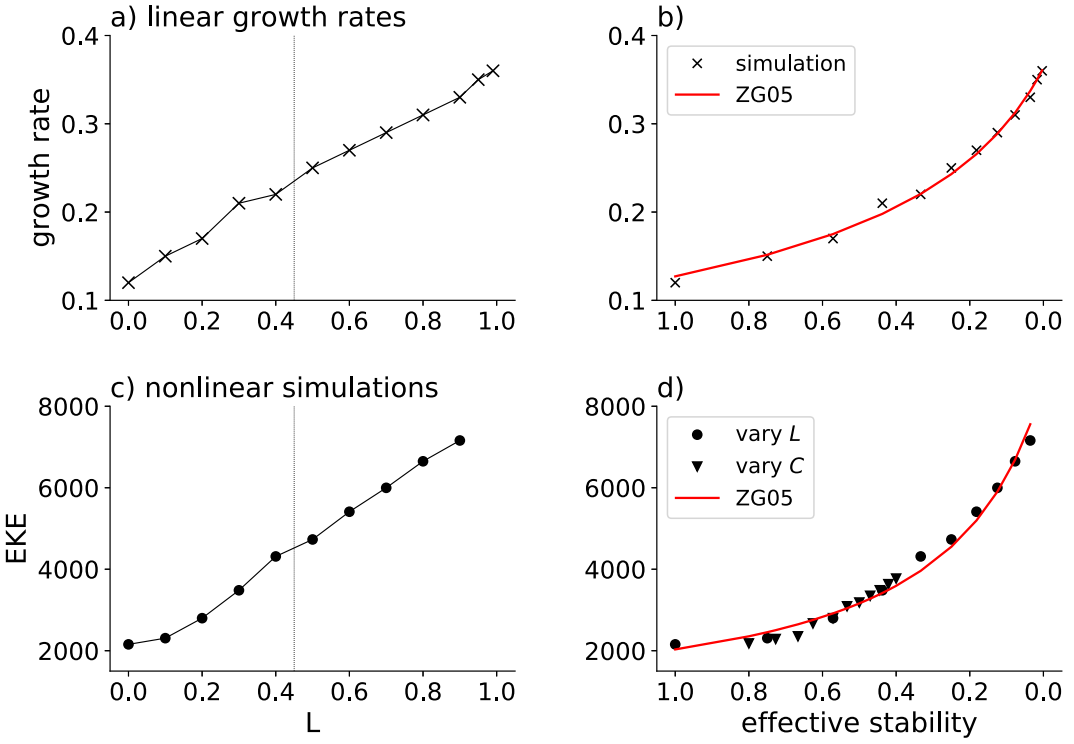

FIG. 1. Results of the homogeneous QG calculations. (top) Eddy linear growth rates (a) as a function of L and (b) as a function of the effective stability r. The red curve shows the growth rates predicted by Eq. (4) multiplied by a constant obtained by linear least squares regression. (bottom) Domain-averaged EKE in the nonlinear simulations (c) as a function of L and (d) as a function of effective stability. In (d), the red curve shows the EKE predicted by Eq. (4), assuming eddy length scales stay fixed and with the y-offset and multiplicative constant obtained by least squares linear regression. The triangles show the results of simulations with C varied and L kept fixed at 0.2. The dotted lines in the left panels mark the transition from the "weak" to "strong" moisture regimes.

introduction, a qualitatively different climate state to the dry and "weak moisture" climates, but the σ^2 scaling appears to hold robustly across the transition. The good match between the σ^2 scaling and the simulated EKEs is somewhat surprising as both Lapeyre and Held (2004) and Brown et al. (2023) found the inverse cascade extending to larger scales as the model is moistened. This suggests that changes in the size of energy-containing eddies are small compared to the changes in σ^2.

These simulations demonstrate that when baroclinicity is fixed linear growth rates and EKE increase when moisture is added to the moist QG model, closely following the scaling derived by Zurita-Gotor (2005). Hence, for fixed environmental conditions, moisture increases the EKE of QG systems.

3. Channel quasigeostrophic model

a. Model description

The channel QG model was described in Lutsko and Hell (2021). It also consists of two constant density layers on a β plane, but the interface between the layers is relaxed to a baroclinically unstable radiative-equilibrium slope, producing a strong zonal jet in the center of the domain. Sponges at the meridional boundaries damp eddy activity, creating a channel geometry.

The nondimensionalized equations of motion are now written in terms of the total potential vorticity

$$\begin{aligned}&\frac{\partial}{\partial t}Q_k(x,y,t)+J[\Psi_k(x,y,t),Q_k(x,y,t)]\\&\quad=-\frac{1}{\tau_d}(-1)^k[\Psi_1(x,y,t)-\Psi_2(x,y,t)-\Psi_R(y)]\\&\qquad-\frac{1}{\tau_f}\delta_{k2}\nabla^2\Psi_k(x,y,t)+(-1)^kL\mathcal{P}(x,y,t)-\nu\nabla^4Q_k(x,y,t),\end{aligned}\tag{5}$$

where $Q_k=\nabla^2\Psi_k+(-1)^k(\Psi_1-\Psi_2)+\beta y$, τ_d is a Newtonian relaxation time scale, and Ψ_R is the radiative-equilibrium interface slope, defined as

$$-\frac{\partial\Psi_R}{\partial y}=\mathrm{sech}^2(y/\sigma),\tag{6}$$

where σ controls the width of the jet and is set to 3.5 in all simulations.

The channel model tracks a single moisture variable $\mathcal{M}$:

$$\begin{aligned}&\frac{\partial}{\partial t}\mathcal{M}(x,y,t)+J[\Psi_2(x,y,t),\mathcal{M}(x,y,t)]\\&\quad=\mathcal{E}(x,y,t)-\mathcal{P}(x,y,t)-\nabla\cdot\mathbf{u}_2(x,y,t),\end{aligned}\tag{7}$$

where $\mathcal{E}$ and $\mathcal{P}$ represent the total evaporation and precipitation, rather than anomalies. Precipitation resets $\mathcal{M}$ to the saturation mixing ratio $\mathcal{M}_s\equiv C(\Psi_1-\Psi_2)$ wherever $\mathcal{M}>\mathcal{M}_s$:

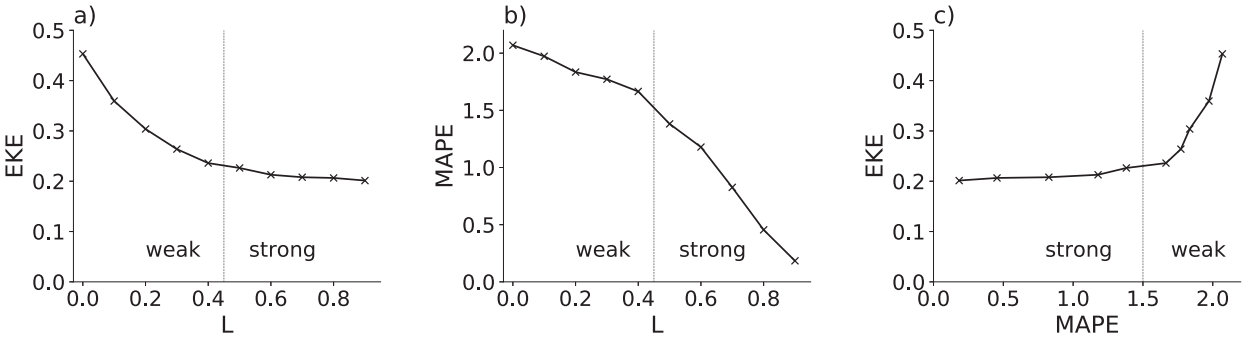

FIG. 2. (a) EKE as a function of L in the moist QG channel simulations. (b) MAPE as a function of L in the same simulations. (c) EKE as a function of domain-averaged MAPE in the same simulations. Both the EKE and the MAPE are calculated by averaging over the baroclinic regions of the simulations (see text for more details). The dotted lines mark the transition from the weak to strong moisture regimes, as indicated by the text on each panel.

$$\mathcal{P} = \begin{cases} (\mathcal{M} - \mathcal{M}_s)/\tau_p, & \text{if } \mathcal{M} > \mathcal{M}_s, \\ 0 & \text{if } \mathcal{M} \le \mathcal{M}_s, \end{cases} \tag{8}$$

with τ_p set to 1 model time unit, and evaporation is calculated using a "bulk formula" wherever the moisture is subsaturated:

$$\mathcal{E} = \begin{cases} \hat{\mathcal{E}}|\mathbf{U}_2|(\mathcal{M}_s - \mathcal{M}), & \text{if } \mathcal{M} < \mathcal{M}_s, \\ 0 & \text{if } \mathcal{M} \ge \mathcal{M}_s, \end{cases} \tag{9}$$

with $|\mathbf{U}_2|$ being the absolute wind speed in the lower layer and $\hat{\mathcal{E}}$ being a constant of proportionality.

We use the same model parameters and domain size as Lutsko and Hell (2021): The zonal width is 72 units and the meridional length is 96 units, with 128 wavenumbers retained in both dimensions. For the parameters not related to moisture, we set $\beta = 0.2$, $\tau_f = 15$, $\tau_d = 100$, and $\nu = 10^{-6}$. For the moist parameters, we set $C = 2$ and $\hat{\mathcal{E}} = 0.1$ and then vary L from 0 to 0.9. We note that these moist parameters correspond to slightly different dimensional values than in the homogeneous model as, for simplicity, we have set $m_0 = 10$ g kg^{-1}, whereas Lapeyre and Held (2004) used an estimate of m_0 from observations. Furthermore, a smaller length scale and a faster wind speed were used in the nondimensionalization, so 1 time unit $\approx$ 0.2 Earth days in the channel QG simulations.

b. Simulation results

The channel model exhibits the opposite behavior to the homogeneous model, as the EKE decreases monotonically with L, from 0.46 in the dry case to just over 0.2 in the $L = 0.9$ case (Fig. 2a; the EKE $= \sum_k \langle u_i'^2 + v_i'^2 \rangle$, where angled brackets denote a time and horizontal average).[2] The largest decreases occur for $L < 0.4$, and the EKE only decreases slightly between $L = 0.5$ and $L = 0.9$. To understand the relationship between L and EKE in these simulations, we examine the terms in the Lorenz energy cycle (Lorenz 1955, appendix A), especially the MAPE (defined in appendix A). If the (dry) supercriticality of the channel model is assumed fixed, then the MAPE should be linearly related to the EKE (Schneider and Walker 2006).

The MAPE also decreases monotonically with L (Fig. 2b); but whereas the EKE is roughly constant at large L, the MAPE decreases more rapidly in the strong moisture regime ($L > 0.4$). Figure 2c shows that EKE is essentially independent of the MAPE in the strong moisture regime (the transition between the weak and strong moisture regimes can be diagnosed by examining the power spectra of EKE, as the spectra exhibit maxima at the typical scale of the lower-layer cyclones for large L). Brown et al. (2023) suggest that the moist criticality may be more relevant for baroclinic adjustment than the dry criticality and that the dry criticality should decrease as the meridional moisture gradient increases. Consistent with their arguments, we find that the dry criticality is not fixed and decreases with L (not shown), which may explain the highly nonlinear relationship between MAPE and EKE in these simulations.

The qualitative change in the relationship between EKE and MAPE near $L = 0.4$ motivates us to examine the weak and strong moisture simulations separately. In the weak moisture regime, the MAPE decreases with increasing L because precipitation tends to form on the poleward side of the jet [Fig. 3a; see also Fig. 1 of Lutsko and Hell (2021)]. Latent heat is released where the model is relatively cool, weakening the meridional temperature gradient (Fig. 3b) and lowering the MAPE. This is the primary reason for the reduction in EKE with L, but there is also a notable decrease in EKE between the dry and $L = 0.1$ cases—more than would be expected from a linear regression of MAPE onto EKE in this regime. We have traced the additional decrease to precipitation's role as a sink of MAPE when latent heating is weak (crosses in Fig. 4b), reducing the conversion to EAPE compared to the dry case. Precipitation was also a sink of MAPE in the comparison of dry and moist shallow water simulations in Bembenek et al. (2020). It contributes weakly to the EAPE budget for small L, which Bembenek et al. (2020) showed is

[2] We have calculated all energy budget terms in the channel QG simulations by averaging over the baroclinic zone, which we define as where the lower-layer mean PV gradient is negative. We obtain similar results when averaging over the whole domain but prefer to restrict our focus to the baroclinic zone to avoid the sponge regions at the edges of the domain. Bembenek et al. (2020) calculated their energy budgets using global integrals.

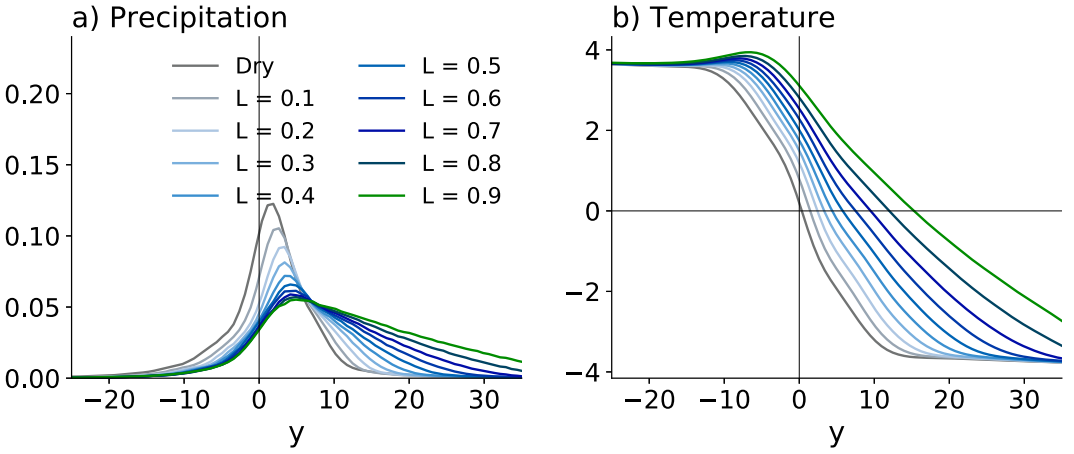

FIG. 3. (a) Climatological zonal-mean precipitation in the moist channel simulations. (b) Climatological zonal-mean temperature ($\Psi_1 - \Psi_2$) in the moist channel simulations.

due to precipitation being out of phase with temperature in this regime.

In the strong moisture regime, both precipitation terms are sources of potential energy (crosses in Fig. 4), and the leading balance in the MAPE budget is between precipitation and radiation. In this regime, the combination of latent heating and eddy heat fluxes causes the model to be anomalously warm at latitudes up to $y = +20$ (Fig. 3b), but the largest temperature gradients are still at relatively low latitudes [e.g., the jet is centered near $y = +5$; see Lutsko and Hell (2021)], so the majority of eddy activity is in the relatively warm region between $y = 0$ and $+20$. Most of the precipitation also occurs in these latitudes, and the associated latent heat release now heats a relatively warm region.

These simulations resemble a climate in which the strongest temperature gradients are located in the warm subtropics, as are the eddy-driven jet and the majority of the eddy activity. Higher latitudes have relatively weak temperature gradients and are quiescent compared to the subtropics, though passing storms occasionally bring precipitation. The MAPE budget is a balance between latent heat release warming the subtropics and increasing the MAPE and radiation cooling the subtropics and acting as a sink of MAPE. A small residual is left over to be converted into EAPE, and this residual saturates for strong latent heating, so the energy available to be converted into EKE is roughly constant for $L \geq 0.5$.

Precipitation becomes a source of EAPE in the strong moisture regime (Fig. 4b), as latent heat is released in the cores of the warm cyclones that dominate these climates, but this term is small compared to precipitation's zonal-mean contribution. We have not investigated the cyclones in further detail, but note they resemble the diabatic Rossby vortices described by Moore and Montgomery (2005) (see also Kohl and O'Gorman 2022).

4. Moist gray radiation model

a. *Model description*

The moist, gray radiation GCM was first described by Frierson et al. (2006). It solves the primitive equations on the sphere and

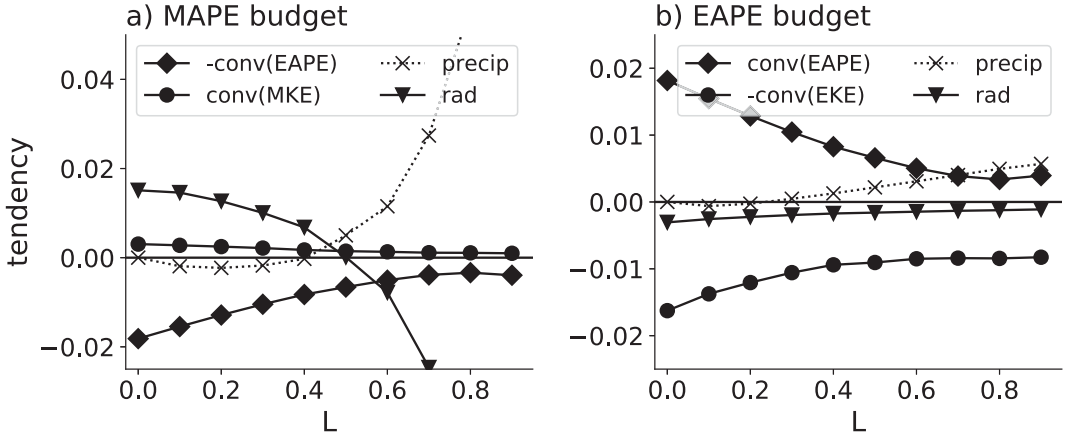

FIG. 4. (a) Terms in the MAPE budget of the moist QG channel simulations. (b) Terms in the EAPE budget of the moist QG channel simulations. Note the different y-axis scales.

is forced by a gray radiation scheme. The GCM is coupled to a slab ocean of depth 1 m, with no representation of ocean dynamics or sea ice, and the model includes the simplified Betts–Miller (SBM) convection scheme of Frierson (2007). A mixed-layer depth of 1 m was used so that the model would spin up quickly, while leaving the resulting mean climate the same as for larger mixed-layer depths. We show results using a convective relaxation time scale τ_{SBM} of 2 h and a reference relative humidity $\text{RH}_{\text{SBM}} = 0.7$. The boundary layer scheme is the one used by O'Gorman and Schneider (2008a). In every experiment, the GCM was integrated at T85 truncation (corresponding to a resolution of roughly 1.4° × 1.4° on a Gaussian grid) with 30 vertical levels extending up to 16 hPa, starting from a state with uniform SSTs.

To vary moisture in the model, we follow Frierson et al. (2006) and multiply the saturation vapor pressure by a constant factor γ:

$$e_s^*(T, \gamma) = \gamma e_{s0}^*(T), \tag{10}$$

where e_{s0}^* is the model's default saturation pressure. We ran an initial set of simulations with γ varied from 0 (i.e., the model is dry) to 1 in increments of 0.2; then, motivated by a desire to further probe the dry–moist transition, we ran an additional set of simulations with γ set to 10^{-3}, 10^{-2}, and 10^{-1}. All simulations were run for 2000 days, with averages taken over the final 1500 days, and we will present simulations with equinoctial solar forcing, so all data are symmetrized about the equator.

b. Calculating the MAPE

We calculated the dry MAPE following the original formulation in Lorenz (1955), but this is difficult to interpret, so we also used an approximate form of Lorenz's dry MAPE derived by Schneider and Walker (2008) that allows the drivers of changes in MAPE to be diagnosed:

$$\text{MAPE} \approx \frac{c_p}{24g}\langle \overline{p}s - \overline{p}_t\rangle \Gamma \langle \partial_y \overline{\theta}\rangle^2 L_z^2, \tag{11}$$

where c_p is the heat capacity of dry air, g is the gravitational acceleration, p_s is the surface pressure, p_t is the pressure of the tropopause, θ is the potential temperature, and L_z is the width (in units m) of the baroclinic zone. The term Γ represents an inverse stability:

$$\Gamma = -\frac{\kappa}{p_0}\langle \overline{\partial_p \theta}\rangle^{-1}, \tag{12}$$

where $\kappa = R_d/c_p$, with R_d being the dry gas constant and p_0 a reference pressure. Overbars denote time averages, and angle brackets now denote averages over the "baroclinic zone." We set $c_p = 1005$ J kg^{-1} K^{-1}, $g = 9.8$ m s^{-2}, $\kappa = 2/7$, and $p_0 = 1000$ hPa in all calculations.

There is ambiguity over whether the terms involving potential temperature should be evaluated in the lower troposphere only or over the depth of the entire troposphere. Schneider and Walker (2008) originally suggested taking lower-tropospheric values (e.g., averages over 800–700 hPa), but O'Gorman and Schneider (2008b) later proposed averaging over the depth of the troposphere to account for latent heat release aloft. As discussed below, in the dry simulations the horizontal temperature gradients go to zero in the upper troposphere, suggesting the lower tropospheric MAPE may be a more appropriate measure of MAPE. For this reason, we have used the lower-tropospheric form for interpretation, though both methods give qualitatively similar results. For other simulations, designed to investigate global warming, for example, taking a vertical integral may be more appropriate.

There is also ambiguity as to how to define the baroclinic zone. Schneider and Walker (2006) defined it as the region where the eddy potential temperature flux at 840 hPa is within 30% of its maximum, whereas O'Gorman and Schneider (2008b) suggested defining it as the latitudes within 15° of the maximum vertically integrated eddy potential temperature flux. We have calculated the EKE and the MAPE using both definitions and find that our results are qualitatively insensitive to this choice (not shown), and the results presented here use the Schneider and Walker (2006) definition but with the threshold set to 50%, which gives more robust estimates. The baroclinic zone thus defined typically extends from ~22° to 70° and shifts poleward slightly as the model is moistened—interestingly, the jets in both the QG model and the GCM move poleward as moisture is added (Frierson et al. 2006; Lutsko and Hell 2021). Appendix B shows the EKE and MAPE in the GCM simulations calculated using global integrals, as done by, e.g., Kim and Kim (2013), for comparison.

c. EKE across climates

As in the channel QG model simulations, the EKE decreases as the GCM transitions from dry to moist, from almost 1 MJ m^{-2} in the dry case to ~0.8 MJ m^{-2} for $\gamma = 1$ (Fig. 5a). The decrease is roughly exponential in γ, and the EKE appears to saturate for large γ. We investigate these changes first by comparing them with changes in MAPE and then by examining the terms in the Lorenz energy cycle in the simulations.

1) EKE AND MAPE

In the GCM simulations, the MAPE also decreases exponentially with γ, from over 10 MJ m^{-2} in the dry simulation to just over 2.5 MJ m^{-2} for $\gamma = 1$ (Fig. 5b). Plotting the EKE against the MAPE reveals the existence of two regimes: a "dry" regime and a "moist" regime, with the transition near $\gamma = 0.2$ (Fig. 5c). In each regime, the EKE is roughly linear in MAPE, but the slope is substantially smaller in the dry regime (i.e., the EKE increases more slowly for a given change in MAPE), suggesting that MAPE is converted into EKE less efficiently in the dry regime.

We return to the transition between the dry and moist regimes below and focus first on understanding the changes in MAPE. The approximate MAPE allows us to identify what causes the MAPE to decrease as moisture is added to the model. Comparing the terms in Eq. (11) shows that the most important factor is the inverse stability Γ, with the meridional surface temperature gradient a secondary contributor to decreases in MAPE as the model is moistened (Fig. 5d).

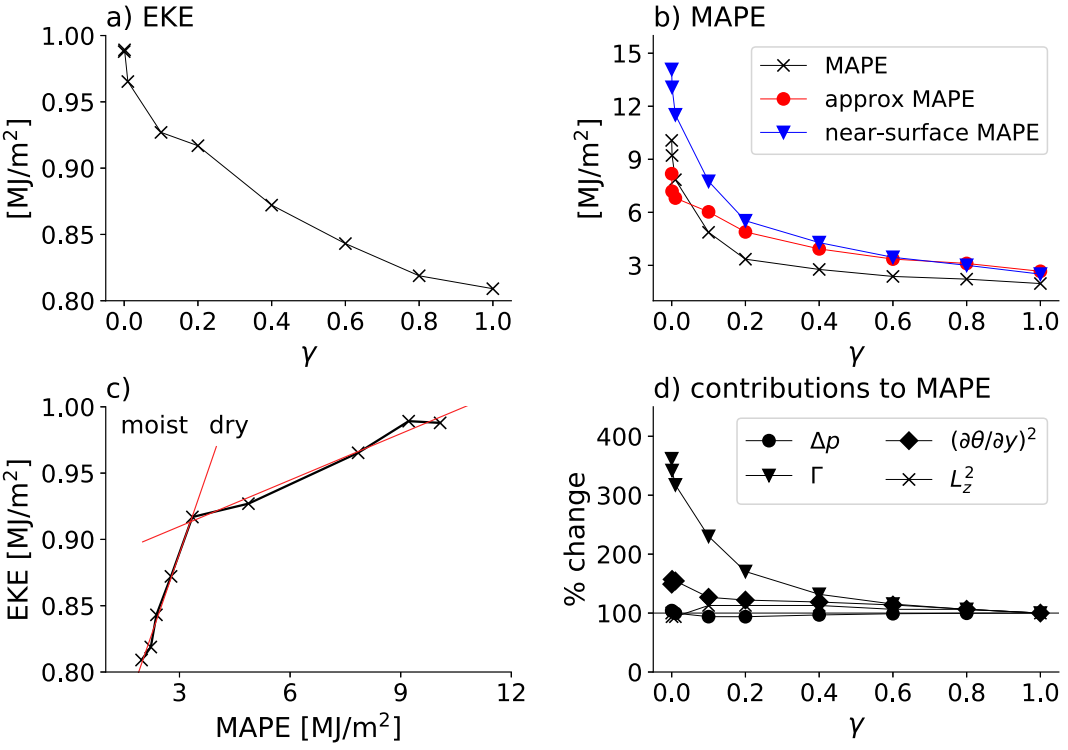

FIG. 5. (a) EKE as a function of γ in the moist GCM simulations. (b) MAPE as a function of γ in the moist GCM simulations. The black crosses show the true MAPE, the red circles show the approximate MAPE [Eq. (11)] with terms calculated by integrating over the depth of the troposphere, and the blue triangles show the approximate MAPE with terms calculated using near-surface values. (c) EKE vs MAPE in the same simulations. The vertical black dashed line approximately separates the moist and dry regimes, based on MAPE and EKE, and the solid red lines show linear least squares fit to the data in the two regimes. (d) Contributions of different terms in Eq. (11) to the near-surface approximate MAPE in the same simulations [blue triangles in (b)], with each term normalized by its value for $\gamma = 1$.

Examining the climatological potential temperature in the initial six simulations confirms the stability increases as moisture is added to the model (Fig. 6): In the dry case, the isentropes are vertical in most of the midlatitude troposphere, and they become more sloped as moisture is added. We also note that the meridional temperature gradients go to zero in the upper troposphere of the driest simulations (see, e.g., near 400 hPa in the top left of Fig. 6), suggesting that it is inappropriate to integrate over the full troposphere when calculating the MAPE.

The vertical isentropes in the dry simulation imply that the stability in much of the midlatitudes is largely set by convection, as was noted by Frierson et al. (2006). We have experimented with strengthening the midlatitude baroclinicity by increasing the parameter controlling the equator-to-pole insolation gradient Δ_s (Frierson et al. 2006) from 1.4 to 1.8, but even in this setup the isentropes are essentially vertical in the midlatitudes of a dry simulation (not shown). We are unsure how to avoid producing vertical isentropes in dry simulations, but note that Schneider and O'Gorman (2008) found that extratropical stratification scales with convective lapse rate in a dry model, even when the stability is clearly set by eddy fluxes (see their Fig. 4). The decrease in the meridional temperature gradient is also large enough that even without the stability changes, the EKE would decrease in moister climates (diamonds in Fig. 5d), giving confidence that these results are not artifacts of the GCM's convection scheme.

2) LORENZ ENERGY CYCLE

The results of the previous section indicate that increases in stability are the primary cause of the reductions in EKE as moisture is added to the GCM but also demonstrate the limitations of using MAPE to explain EKE variations. In both regimes, the linear fit is approximate, and the very weak stabilities in the dry simulations may push beyond the bounds in which the concept of MAPE is appropriate. As an alternative approach to understanding the changes in EKE, we examine the terms in the Lorenz energy cycle, particularly the diabatic terms associated with latent heat release, radiative cooling, and surface fluxes. While the Lorenz energy cycle has been well studied in idealized models and reanalysis data (e.g., Li et al. 2007; Kim and Kim 2013; Chai et al. 2016; Pan et al. 2017; Lembo et al. 2019), the diabatic terms have received relatively little attention (though see Romanski and Rossow 2013). These are calculated as (Lorenz 1955) follows:

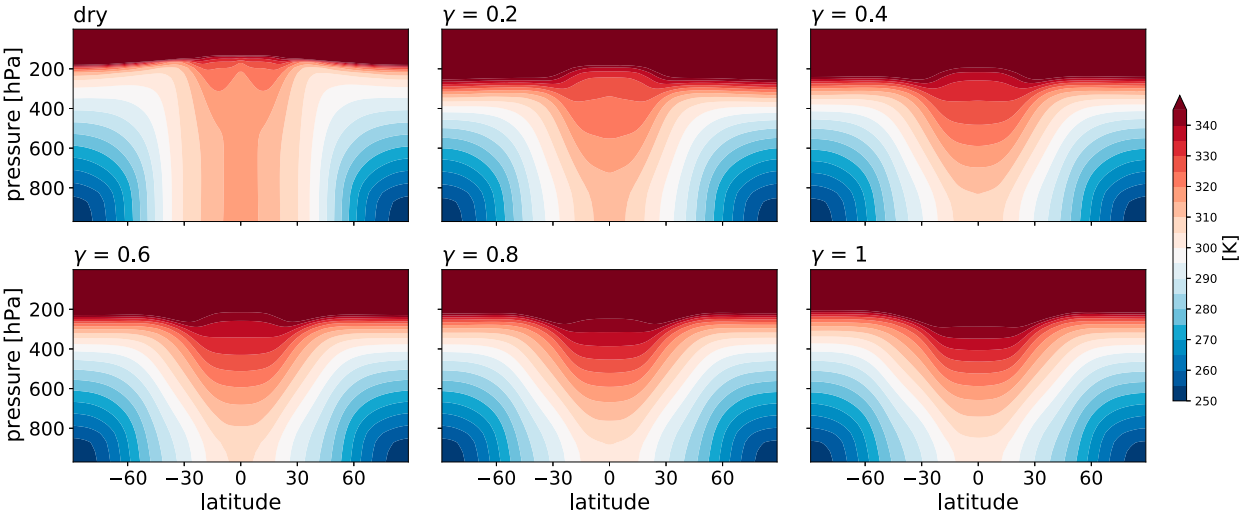

FIG. 6. Climatological zonal-mean potential temperatures as a function of latitude and pressure in the six moist GCM simulations with γ varied in increments of 0.2.

$$G_Z = \frac{-1}{g}\int_0^{p_s}\left(\frac{p_s}{p}\right)^{\kappa}\Gamma\langle\overline{T^*Q^*}\rangle dp, \tag{13a}$$

$$G_E = \frac{-1}{g}\int_0^{p_s}\left(\frac{p_s}{p}\right)^{\kappa}\Gamma\langle\overline{T'Q'}\rangle dp, \tag{13b}$$

where Q denotes a diabatic heating, asterisks denote stationary anomalies from the time and meridional averages, primes denote transient anomalies, and angle brackets again denote horizontal averages over the baroclinic zone. The term G_Z is the contribution to the MAPE budget, and G_E is the contribution to the EAPE budget. We have calculated the contribution of atmospheric latent heating $G_{Z,P}$ and $G_{E,P}$ explicitly and the contribution of diabatic terms not associated with atmospheric latent heating ($G_{Z,\mathrm{NP}}$ and $G_{E,\mathrm{NP}}$) implicitly. The latter are the sum of the surface sensible and latent heat fluxes and atmospheric radiative cooling. An important caveat to our results is that the gray radiation assumption produces unrealistic vertical radiative cooling profiles, likely distorting radiation's contributions to $G_{Z,\mathrm{NP}}$ and $G_{E,\mathrm{NP}}$. We reran several of the GCM simulations and output the radiative cooling, finding that it contributes 25%–35% of the total $G_{Z,\mathrm{NP}}$. We believe this is a small enough contribution for our results to be qualitatively robust to the use of more realistic profiles, though changes in radiative cooling may shift where the transition from dry to moist occurs.

The MAPE and EAPE budgets are plotted as functions of γ in Fig. 7. For $\gamma \geq 0.1$, the diabatic terms are the largest terms in the MAPE budget, with atmospheric latent heating being a strong source of MAPE and the other terms combining to form a strong sink of MAPE. The conversions to EAPE and from zonal kinetic energy (ZKE) balance the net diabatic heating and are substantially smaller than the individual diabatic terms. These results are generally consistent with the observational analysis of Romanski and Rossow (2013), as well as the balance seen in the strong moisture QG simulations. For smaller values of γ, $G_{Z,P}$ is negligible and $G_{Z,\mathrm{NP}}$ is a source of MAPE, reflecting strong surface sensible heat fluxes

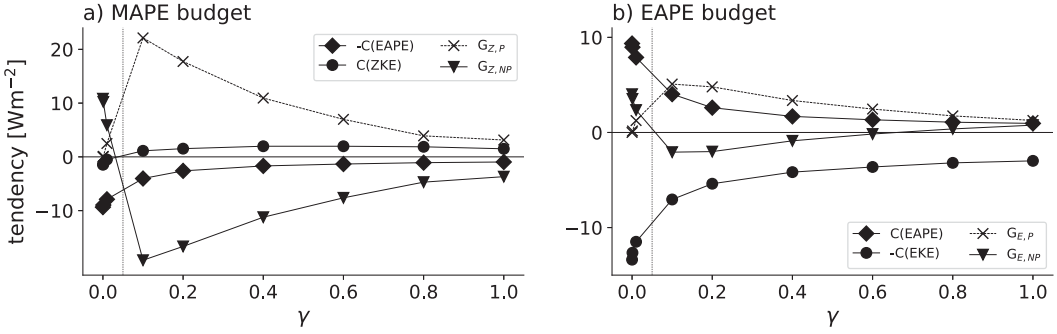

FIG. 7. (a) Terms in the MAPE budget of the moist GCM simulations. (b) Terms in the EAPE budget of the moist GCM simulations. The terms $G_{Z,\mathrm{NP}}$ and $G_{E,\mathrm{NP}}$ denote contributions from diabatic heating not associated with latent heat release, which are calculated as residuals. Note the different y-axis scales. The dashed vertical lines in both panels separate the moist and dry regimes, now defined in terms of whether latent heat fluxes or sensible heat fluxes drive the circulation.

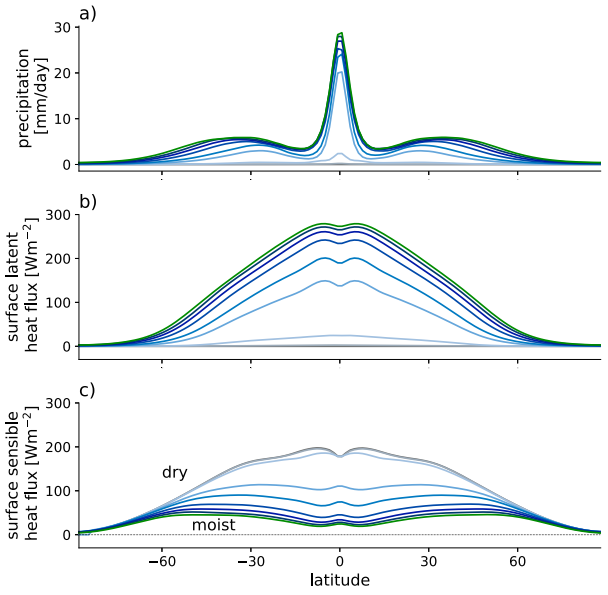

FIG. 8. (a) Climatological surface precipitation in the moist GCM simulations. (b) Climatological surface latent heat flux in the moist GCM simulations. (c) Climatological surface sensible heat flux in the moist GCM simulations. Note that in all three panels the dry simulation and the $\gamma = 10^{-3}$ simulation generally plot on top of each other.

at low latitudes (see Fig. 8) that win out over the surface latent heat fluxes and cooling by radiation. The conversion to EAPE balances the generation of MAPE by surface heating. These results suggest a transition from the dry to moist regimes between $\gamma = 0.01$ and $\gamma = 0.1$, when atmospheric latent heating replaces surface sensible heating as the dominant source of MAPE. We discuss the dry-to-moist transition further in the next section.

It is surprising that the atmospheric latent heating contribution weakens as the atmosphere moistens. Examining the zonal-mean atmospheric latent heating shows that this is a consequence of the migration of the location of the maximum extratropical condensation to higher latitudes as γ is increased (Fig. 9; Fig. 8a shows that the midlatitude precipitation maximum also moves to higher latitudes). For example, in the $\gamma = 0.2$ case, the maximum heating is found in the subtropics, where the atmosphere is already warm, whereas in the $\gamma = 1$ case, the latent heating maximizes near 42°, where the atmosphere is relatively cool (cf. middle panel of the top row and rightmost panel of the bottom row in Fig. 9). We are currently investigating the poleward shift of condensational heating, but note here that most evaporation still occurs in the subtropics (Fig. 8b), so the shift in the location of maximum atmospheric latent heating is the result of an increase in the distance water vapor is transported before it condenses out [or since its "time of last saturation"; Pierrehumbert et al. (2007), Sherwood et al. (2010)] as γ is increased. This could be related to changes in near-surface relative humidity or to the trajectories of individual air parcels. We have not investigated the condensational heating in detail, though we have confirmed that the subtropical near-surface relative humidity is higher for small γ, so parcels of water vapor carried on the same trajectory condense out sooner than for large γ.

The MAPE budget thus provides a different perspective on the reduction in EKE with γ and on the dynamics of the midlatitudes more generally. The dry regime corresponds to the conventional picture of the atmosphere's circulation, in which low latitudes are warmed, mainly through surface sensible heat fluxes, and this generates kinetic energy. But when a small amount of moisture is added to the GCM (~10% of the moisture in the control climate), the sensible heat flux drops, and atmospheric latent heat release becomes the leading term generating MAPE, balanced by atmospheric radiative cooling and surface turbulent fluxes. Thinking of the atmosphere as a heat engine driven by the temperature difference between where energy is input and where it is radiated away, adding moisture decreases the atmosphere's thermodynamic

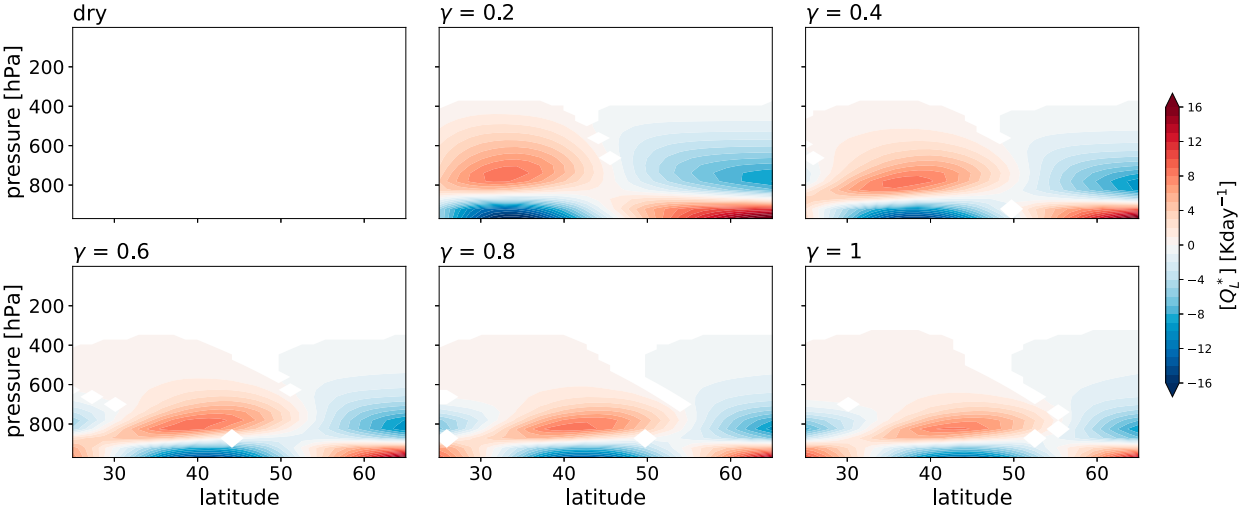

FIG. 9. Anomalous zonal-mean latent heating (Q_L^*) in the six moist GCM simulations with γ varied in increments of 0.2.

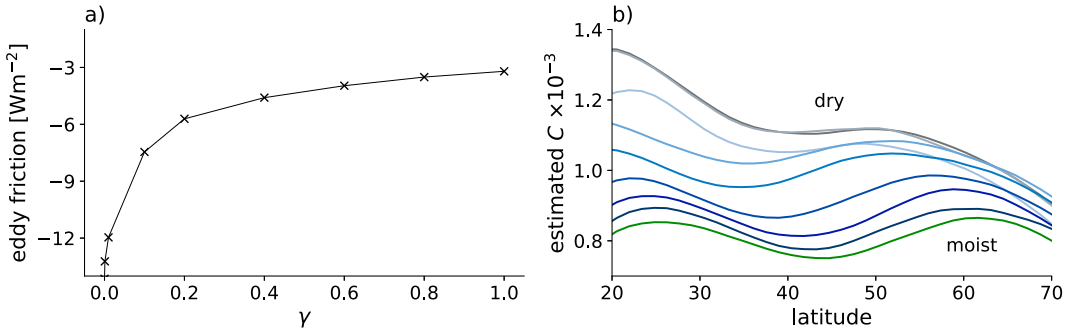

FIG. 10. (a) Sink of EKE due to eddy friction in the moist GCM simulations. (b) Effective drag coefficients C in the moist GCM simulations, diagnosed from the time- and zonal-mean surface fluxes. The term γ increases going from the dark gray curve (labeled dry) to the green curve (labeled moist). The dry simulation and the $\gamma = 10^{-3}$ simulation plot on top of each other.

efficiency (it decreases this temperature difference) because energy is input at the dewpoint temperature of the near-surface subtropical air, rather than at the surface temperature (see also Romps 2008; Pauluis 2011; Bannon 2015). For $\gamma = 0.1$, moisture condenses close to where it is evaporated, and the climate is functionally similar to a dry atmosphere in which heat is input at the surface through sensible heat transfer (i.e., the subtropical dewpoint temperature is close to the near-surface temperature). For large values of γ, the moisture is transported a significant distance and the temperature difference is smaller.

Finally, $G_{E,P}$ is a source of potential energy (Fig. 7b), consistent with Chang et al. (2002). In the moist regime, the conversion from MAPE to EAPE is roughly the same magnitude as $G_{E,P}$, and these together are balanced by the conversion to EKE. Interestingly, $G_{E,\mathrm{NP}}$ switches from being a sink of EAPE for small γ to a source for $\gamma > 0.6$. As with the $G_{Z,\mathrm{NP}}$ term in the MAPE budget, this likely reflects an increased importance of the surface sensible heat flux.

d. *The transition to the dry limit*

The previous two sections identify different definitions of the dry-to-moist transition. The relationship between EKE and MAPE exhibits a break between $\gamma = 0.1$ and $\gamma = 0.2$, where the slope changes, while the MAPE budget suggests the transition occurs for $\gamma < 0.1$, when atmospheric latent heating takes over as the leading driver of the circulation. The former emphasizes differences in the efficiency with which the atmosphere converts MAPE into EKE, while the latter focuses on the driver of the flow, even if the impact on EKE is similar.

Both definitions of the transition are associated with the Bowen ratio:

$$\mathrm{Bo} \equiv \frac{\text{sensible heat flux}}{\text{latent heat flux}}. \tag{14}$$

When Bo = 1, the MAPE budget largely consists of a balance between atmospheric latent heating and radiative cooling, so the dry-to-moist transition must occur for Bo greater than 1, when sensible heat fluxes can be the main source of MAPE. Comparing Figs. 8b and 8c shows that Bo is close to 1 in the $\gamma = 0.1$ simulation, as the maximum surface sensible and latent heat fluxes are both ~150 W m^{-2} in this simulation, consistent with the transition occurring for $\gamma < 0.1$.

The importance of the sensible heat flux in the dry regime also explains the change in the slope of the MAPE–EKE relationship at $\gamma \approx 0.2$. A large sensible heat flux implies a large air–sea temperature difference, which in turn implies stronger surface friction: Monin–Obukhov similarity theory says that the surface drag coefficient depends on the stability of the near-surface boundary layer (Troen and Mahrt 1986; Frierson et al. 2006). So, as the model is moistened, the boundary layer stabilizes and surface friction weakens, becoming a weaker sink of EKE. We confirm this in Fig. 10a, which shows the frictional contribution to the EKE budget in the GCM simulations, calculated as a residual from the EKE budget. The sink of EKE decreases exponentially in magnitude with γ, partly due to smaller effective drag coefficients (Fig. 10b) and also because the surface winds weaken. The smaller coefficients cause a change in the MAPE–EKE slope near $\gamma = 0.2$, though the Bowen ratio is less than 1. Modifying the surface drag, for example, by changing the surface roughness, could alter where the transition from the dry to moist regimes occurs.

5. Conclusions

In this study, we have sought to reconcile previous work showing that moisture can both increase and decrease midlatitude EKE. We have done this by arguing that moisture increases the growth rates of individual eddies but makes the large-scale environment for eddy growth less favorable. For climates like the present day, the latter effect wins out, and moisture decreases atmospheric EKE.

We have demonstrated this point using simulations with a hierarchy of idealized atmospheric models. First, we have used a moist QG model in homogeneous and channel configurations. When baroclinicity is fixed, adding moisture increases linear eddy growth rates and increases the EKE of nonlinear simulations. Both changes closely follow the scaling of Zurita-Gotor (2005), which predicts that the growth rate decreases with effective stability. In the channel configuration, the baroclinicity is free to evolve and the EKE decreases as moisture is added. In simulations with weak latent heating, the EKE

decreases because precipitation mostly forms on the poleward side of the jet, releasing latent heat where the model is relatively cold and decreasing the MAPE. When latent heating becomes a more important part of the model's thermodynamic budget, the energetics change considerably, becoming a balance between latent heat release (which is now a source of MAPE) and radiative cooling (which is a sink of MAPE). In this large-scale "radiative–convective equilibrium," EKE production is a small residual and saturates as the strength of the latent heating is further increased.

Next, we examined dry and moist simulations with an idealized GCM. In this model, EKE also decreases as moisture is added,[3] consistent with decreases in the MAPE. The MAPE decreases as the model is moistened because the midlatitude stability increases and, to a lesser extent, because of weakened meridional temperature gradients. We have also interpreted the changes in EKE using the Lorenz energy cycle, focusing particularly on the diabatic terms in the MAPE budget. This reveals that the energy available to be converted from MAPE to EAPE is a small residual of a large cancellation between atmospheric latent heating, a source of MAPE, and the other diabatic terms (surface sensible and latent heat fluxes and radiative cooling), which are a net sink of MAPE. Surprisingly, these energetics are analogous to those of the strong moisture QG simulations, despite the flow in those simulations not appearing to be very Earth like. The saturation of the EKE as moisture is added to the GCM reflects the migration of atmospheric latent heat release to higher latitudes, where the atmosphere is relatively cooler, resulting in a weaker source of MAPE. These results highlight an important caveat to our study: the generation of available potential energy is sensitive to the vertical profile of longwave absorbers, which is not realistic in a gray radiation model. In dry simulations, with negligible latent heating, EKE is mostly generated by surface sensible heat fluxes in the subtropics, resembling the original description of the atmosphere's energy cycle by Lorenz (1955).

The MAPE–EKE analysis and the Lorenz energy cycle both suggest the presence of two regimes in the GCM. The relationship between MAPE and EKE changes slope near $\gamma = 0.2$, as MAPE is converted into EKE less efficiently in the dry, small γ regime (i.e., the slope shallows), and we also see a transition from surface sensible heat fluxes driving the circulation to atmospheric latent heat fluxes driving the circulation near $\gamma = 0.1$. These transitions are linked, as large sensible heat fluxes reflect large surface to near-surface air temperature gradients, implying a more unstable boundary layer and, in turn, stronger surface friction and a larger sink of EKE.

We have thus shown that the presence of water vapor in Earth's atmosphere makes the midlatitude circulation more sluggish, with weaker eddies and more predictable variability (Lutsko and Hell 2021). While latent heat release plays a crucial role in intensifying individual storms, these storms would be stronger in a dry atmosphere that had an environment more favorable for eddy growth.[4] These results are consistent with studies of changes in midlatitude EKE under warming: Although a warmer atmosphere can hold more water vapor, decreases in meridional temperature gradients and increases in static stability lead to decreases in MAPE and reductions in EKE, as seen here (O'Gorman and Schneider 2008b; Schneider et al. 2010; O'Gorman 2010; Gertler and O'Gorman 2019). EKE also decreases in simulations of climates colder than that of the present-day Earth. O'Gorman and Schneider (2008b) attributed this decrease to a shrinking of the depth of the troposphere (an effect not seen in our simulations), while Shaw and Graham (2020) attributed the decrease to reduced meridional moisture gradients. We note here that Clausius–Clapeyron scaling suggests a global cooling of ~17 K would reduce the mean saturation vapor pressure by 90%, potentially putting the atmospheric circulation in the dry regime identified here. Past snowball Earth states may have been at least this cold (e.g., Pierrehumbert et al. 2011); however, we caution against using our results to compare very different climate states, which likely include other changes, such as in surface albedo, that are not represented in our simulations.

Our analysis has focused on the MAPE and EKE budgets, but an alternative approach to studying atmospheric EKE is to focus on the atmosphere's entropy budget or, relatedly, the work done by the atmosphere (e.g., Pauluis and Held 2002a,b; Pauluis 2007; Pauluis et al. 2008; Romps 2008; Raymond 2013; Laliberté et al. 2015; Chang and Held 2022). We have avoided this approach because there is ambiguity with how to define the terms in the moist GCM's entropy budget, especially those associated with artificial sources and sinks of entropy found in any numerical model (Raymond 2013), and because the entropy budget can only be used to constrain the total (zonal-mean plus eddy) kinetic energy of the atmosphere.

Nevertheless, our results qualitatively match the interpretation suggested by focusing on the atmosphere's entropy budget. In this perspective, the total work done by the atmospheric circulation is determined by the atmosphere's heat engine efficiency and a "Gibbs penalty," representing thermodynamic inefficiencies due to phase changes of water vapor (Pauluis 2011; Singh and O'Neill 2022). The atmosphere's heat engine efficiency decreases with more water vapor, as the temperature at which the atmosphere emits energy to space is roughly constant with γ, while the input temperature decreases with γ: In a dry climate, energy is mainly input through surface sensible heat exchange in the subtropics, while in moist climates, energy is input through condensation at higher altitudes (see also discussion in Pauluis and Held 2002b). Similarly, the Gibbs penalty required to power the hydrologic cycle should increase with γ. We expect this penalty to have a linear contribution from increasing γ at fixed relative humidity and an additional contribution because the

[3] Note that Fig. 7 of O'Gorman (2011) shows that latent heat release increases the EKE in simulations with a dry version of this GCM with fixed zonal-mean fields.

[4] We have verified that in both the QG model and the GCM individual storms weaken as moisture is added, in addition to the zonal-mean EKE.

free tropospheric relative humidity decreases as the GCM is moistened[5] leading to more entropy production from the diffusion of water vapor (Pauluis 2011). Hence, we expect the Gibbs penalty to increase faster than linearly in γ, further reducing the thermodynamic efficiency. The entropy budget perspective is thus consistent with our results, and these considerations give us confidence in the generality of our findings, despite the unrealistic use of a gray radiation scheme and our neglect of shortwave absorption.

To close, we discuss two implications of our results. First, the comparison of the moist QG model and the moist GCM highlights two drawbacks of moist QG models: the fixed stratification and the fact that precipitation is localized to the poleward side of the jet. The fixed stratification is a well-known limitation of two-layer QG models, though they can mimic changes in "effective" stability in areas of convection (Lapeyre and Held 2003). It has also been suggested that QG models should guide the development of theories for horizontal eddy fluxes that can then be used outside the QG framework to help determine the midlatitude stability (Held 2008). To our knowledge, the strong localization of precipitation has not been noted before and presents difficulties for linking QG systems to more realistic models. In the weak moisture regime of the QG model, precipitation is a sink of MAPE because it forms where the model is relatively cold, but it is always a source in the moist GCM. The bias in precipitation may also limit the usefulness of the moist QG model for other purposes. For example, the strong localized heating likely affects the position and strength of the jet, making it difficult to use the model to study jet dynamics. We note, however, that the jets in both models are pushed poleward as moisture is added, an effect we are currently investigating.

A second implication of our results concerns our novel emphasis on the location of latent heat release for driving the midlatitude atmosphere's circulations. Past studies of the Lorenz energy cycle have often calculated diabatic terms as residuals (e.g., Lembo et al. 2019), but we believe the results shown above demonstrate that these terms merit more attention. The importance of latent heat release provides a new way of interpreting past and future changes in the midlatitude atmosphere. For example, changes in EKE as Earth's climate is warmed or cooled could also be explained in terms of the distance water vapor is transported before it condenses and rains out. We intend to explore this and related questions, building on the analysis of the moist GCM's energy budget presented above.

Acknowledgments. We thank Momme Hell, Pengcheng Zhang, Tiffany Shaw, David Raymond, Isaac Held, and Tim Merlis for feedback on earlier versions of this manuscript; Marty Singh and Morgan O'Neill for helpful discussions about entropy budgets; and three anonymous reviewers and the editor, Bill Boos, for their close readings and constructive comments. We also thank the developers of the Isca climate modeling framework, which was used to run the moist GCM experiments. N. J. L. and J. M.-C. were supported by the National Science Foundation through Grant AGS-2202991.

Data availability statement. The moist QG model used in the first part of the paper is available from https://github.com/nicklutsko/moist_QG_channel. The moist GCM simulations were run with https://execlim.github.io/IscaWebsite/. All analysis scripts are available from: https://github.com/nicklutsko/Moisture_EKE.

APPENDIX A

Available Potential Energy Budgets of the QG Channel Model

In the QG channel model, the MAPE and the EAPE are defined as

$$\text{MAPE} \equiv [\overline{\eta}^2], \tag{A1a}$$

$$\text{EAPE} \equiv [\overline{\eta'^2}], \tag{A1b}$$

where $\eta = \Psi_1 - \Psi_2$ and square brackets denote a time and horizontal average. The MAPE and EAPE budgets are

$$\frac{d}{dt}\text{MAPE} = C(\text{ZKE} \to \text{MAPE}) - C(\text{MAPE} \to \text{EAPE}) + P_z + \text{Rad}_z, \tag{A2a}$$

$$\frac{d}{dt}\text{EAPE} = C(\text{MAPE} \to \text{EAPE}) - C(\text{EAPE} \to \text{EKE}) + P_e + \text{Rad}_e, \tag{A2b}$$

where the conversion terms are

$$\text{ZKE} \to \text{MAPE} = [\overline{\eta}\partial_y(\overline{v_2}\,\overline{\eta})], \tag{A3a}$$

$$\text{MAPE} \to \text{EAPE} = -[\overline{\eta}\partial_y(\overline{v_2'\eta'})], \tag{A3b}$$

$$\text{EAPE} \to \text{EKE} = -[\eta'\nabla\cdot\mathbf{u}_2], \tag{A3c}$$

and the precipitation and radiation terms are

$$P_z = L[\overline{\eta}\,\overline{P}], \tag{A4a}$$

$$P_e = L[\overline{\eta' P'}], \tag{A4b}$$

$$\text{Rad}_z = \frac{1}{\tau_d}[\overline{\eta}(\Psi_R - \overline{\eta})], \tag{A4c}$$

$$\text{Rad}_e = -\frac{1}{\tau_d}[\overline{\eta'^2}]. \tag{A4d}$$

As discussed in the main text, we have calculated all terms in the potential energy budgets of the QG channel model by averaging over regions where the zonal- and time-mean potential vorticity gradients have the opposite signs in the two layers.

[5] Since variations in the evaporative flux into the atmosphere are small for all but the smallest values of γ (Fig. 8b), the partial vapor pressure in the atmosphere is also roughly fixed and the relative humidity decreases with γ.

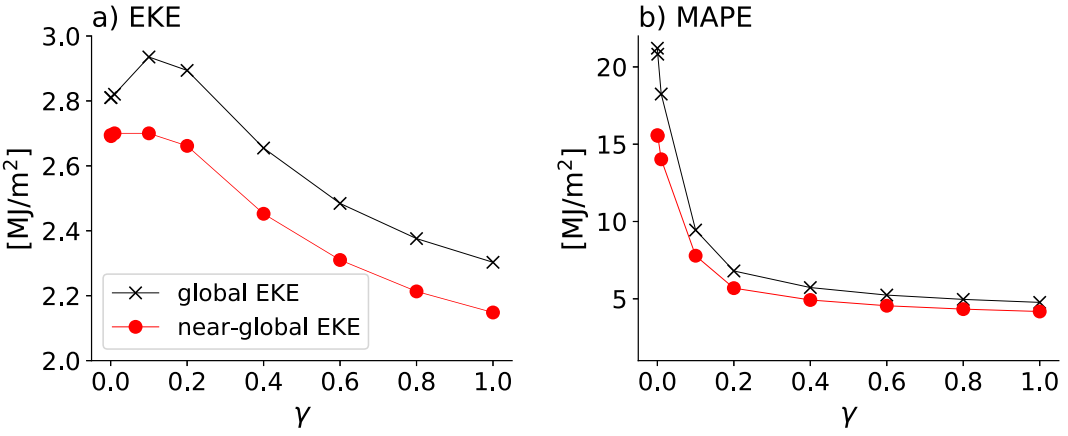

FIG. B1. (a) EKE as a function of γ in the moist GCM simulations. (b) MAPE as a function of γ in the moist GCM simulations. In both panels, black crosses show global integrals taken over all latitudes and the red circles show near-global integrals taken over all latitudes poleward of 10°.

APPENDIX B

Calculating EKE and MAPE with Global Integrals

In the main text, the EKE and MAPE for the GCM simulations are calculated by integrating over the baroclinic zone, following the approach used by Schneider and Walker (2006) and others. We have also calculated EKE and MAPE by taking global integrals, shown in Fig. B1 for the initial set of GCM simulations with γ varied in increments of 0.2. The results are qualitatively similar, except that the EKE in the $\gamma = 0.2$ case is slightly larger than the dry case. The reason for this is that there is very little eddy activity in the deep tropics of the dry simulation, but there is some EKE near the equator in the moist simulations. Excluding latitudes equatorward of ±10° gives results more similar to Fig. 5 in the main text (red circles in Fig. B1).

REFERENCES

Bannon, P. R., 1986: Linear development of quasi-geostrophic baroclinic disturbances with condensational heating. *J. Atmos. Sci.*, **43**, 2261–2274, https://doi.org/10.1175/1520-0469(1986)043<2261:LDOQGB>2.0.CO;2.

——, 2015: Entropy production and climate efficiency. *J. Atmos. Sci.*, **72**, 3268–3280, https://doi.org/10.1175/JAS-D-14-0361.1.

Bembenek, E., D. N. Straub, and T. M. Merlis, 2020: Effects of moisture in a two-layer model of the midlatitude jet stream. *J. Atmos. Sci.*, **77**, 131–147, https://doi.org/10.1175/JAS-D-19-0021.1.

Bischoff, T., and T. Schneider, 2016: The equatorial energy balance, ITCZ position, and double-ITCZ bifurcations. *J. Climate*, **29**, 2997–3013, https://doi.org/10.1175/JCLI-D-15-0328.1.

Bouchut, F., J. Lambaerts, G. Lapeyre, and V. Zeitlin, 2009: Fronts and nonlinear waves in a simplified shallow-water model of the atmosphere with moisture and convection. *Phys. Fluids*, **21**, 116604, https://doi.org/10.1063/1.3265970.

Brown, M. L., O. Pauluis, and E. P. Gerber, 2023: Scaling for saturated moist quasigeostrophic turbulence. *J. Atmos. Sci.*, **80**, 1481–1498, https://doi.org/10.1175/JAS-D-22-0215.1.

Chai, J., M. Jansen, and G. K. Vallis, 2016: Equilibration of a baroclinic planetary atmosphere toward the limit of vanishing bottom friction. *J. Atmos. Sci.*, **73**, 3249–3272, https://doi.org/10.1175/JAS-D-15-0329.1.

Chang, C.-Y., and I. M. Held, 2022: A scaling theory for the diffusivity of poleward eddy heat transport based on Rhines scaling and the global entropy budget. *J. Atmos. Sci.*, **79**, 1743–1758, https://doi.org/10.1175/JAS-D-21-0242.1.

Chang, E. K. M., 2006: An idealized nonlinear model of the Northern Hemisphere winter storm tracks. *J. Atmos. Sci.*, **63**, 1818–1839, https://doi.org/10.1175/JAS3726.1.

——, S. Lee, and K. L. Swanson, 2002: Storm track dynamics. *J. Climate*, **15**, 2163–2183, https://doi.org/10.1175/1520-0442(2002)015<02163:STD>2.0.CO;2.

Emanuel, K. A., M. Fantini, and A. J. Thorpe, 1987: Baroclinic instability in an environment of small stability to slantwise moist convection. Part I: Two-dimensional models. *J. Atmos. Sci.*, **44**, 1559–1573, https://doi.org/10.1175/1520-0469(1987)044<1559:BIIAEO>2.0.CO;2.

Frierson, D. M. W., 2007: The dynamics of idealized convection schemes and their effect on the zonally averaged tropical circulation. *J. Atmos. Sci.*, **64**, 1959–1976, https://doi.org/10.1175/JAS3935.1.

——, I. M. Held, and P. Zurita-Gotor, 2006: A gray-radiation aquaplanet moist GCM. Part I: Static stability and eddy scale. *J. Atmos. Sci.*, **63**, 2548–2566, https://doi.org/10.1175/JAS3753.1.

——, ——, and ——, 2007: A gray-radiation aquaplanet moist GCM. Part II: Energy transports in altered climates. *J. Atmos. Sci.*, **64**, 1680–1693, https://doi.org/10.1175/JAS3913.1.

Gertler, C. G., and P. A. O'Gorman, 2019: Changing available energy for extratropical cyclones and associated convection in Northern Hemisphere summer. *Proc. Natl. Acad. Sci. USA*, **116**, 4105–4110, https://doi.org/10.1073/pnas.1812312116.

Gutowski, W. J., Jr., L. E. Branscome, and D. A. Stewart, 1992: Life cycles of moist baroclinic eddies. *J. Atmos. Sci.*, **49**, 306–319, https://doi.org/10.1175/1520-0469(1992)049<0306:LCOMBE>2.0.CO;2.

Haidvogel, D. B., and I. M. Held, 1980: Homogeneous quasi-geostrophic turbulence driven by a uniform temperature gradient. *J. Atmos. Sci.*, **37**, 2644–2660, https://doi.org/10.1175/1520-0469(1980)037%3c2644:HQGTDB%3e2.0.CO;2.

Held, I. M., 2008: Progress and problems in large-scale atmospheric dynamics. *The Global Circulation of the Atmosphere*, T. Schneider and A. H. Sobel, Eds., Princeton University Press, 1–21.

——, and V. D. Larichev, 1996: A scaling theory for horizontally homogeneous, baroclinically unstable flow on a beta plane. *J. Atmos. Sci.*, **53**, 946–952, https://doi.org/10.1175/1520-0469(1996)053<0946:ASTFHH>2.0.CO;2.

——, and M. Zhao, 2008: Horizontally homogeneous rotating radiative–convective equilibria at GCM resolution. *J. Atmos. Sci.*, **65**, 2003–2013, https://doi.org/10.1175/2007JAS2604.1.

Joos, H., and H. Wernli, 2012: Influence of microphysical processes on the potential vorticity development in a warm conveyor belt: A case-study with the limited-area model COSMO. *Quart. J. Roy. Meteor. Soc.*, **138**, 407–418, https://doi.org/10.1002/qj.934.

Kim, Y.-H., and M.-K. Kim, 2013: Examination of the global Lorenz energy cycle using MERRA and NCEP-reanalysis 2. *Climate Dyn.*, **40**, 1499–1513, https://doi.org/10.1007/s00382-012-1358-4.

Kirshbaum, D. J., T. M. Merlis, J. R. Gyakum, and R. McTaggart-Cowan, 2018: Sensitivity of idealized moist baroclinic waves to environmental temperature and moisture content. *J. Atmos. Sci.*, **75**, 337–360, https://doi.org/10.1175/JAS-D-17-0188.1.

Kohl, M., and P. A. O'Gorman, 2022: The diabatic Rossby vortex: Growth rate, length scale, and the wave–vortex transition. *J. Atmos. Sci.*, **79**, 2739–2755, https://doi.org/10.1175/JAS-D-22-0022.1.

Laîné, A., G. Lapeyre, and G. Rivière, 2011: A quasigeostrophic model for moist storm tracks. *J. Atmos. Sci.*, **68**, 1306–1322, https://doi.org/10.1175/2011JAS3618.1.

Laliberté, F., J. Zika, L. Mudryk, P. J. Kushner, J. Kjellsson, and K. Döös, 2015: Constrained work output of the moist atmospheric heat engine in a warming climate. *Science*, **347**, 540–543, https://doi.org/10.1126/science.1257103.

Lambaerts, J., G. Lapeyre, V. Zeitlin, and F. Bouchut, 2011a: Simplified two-layer models of precipitating atmosphere and their properties. *Phys. Fluids*, **23**, 046603, https://doi.org/10.1063/1.3582356.

——, ——, and ——, 2011b: Moist versus dry barotropic instability in a shallow-water model of the atmosphere with moist convection. *J. Atmos. Sci.*, **68**, 1234–1252, https://doi.org/10.1175/2011JAS3540.1.

——, ——, and ——, 2012: Moist versus dry baroclinic instability in a simplified two-layer atmospheric model with condensation and latent heat release. *J. Atmos. Sci.*, **69**, 1405–1426, https://doi.org/10.1175/JAS-D-11-0205.1.

Lapeyre, G., and I. M. Held, 2003: Diffusivity, kinetic energy dissipation, and closure theories for the poleward eddy heat flux. *J. Atmos. Sci.*, **60**, 2907–2916, https://doi.org/10.1175/1520-0469(2003)060<2907:DKEDAC>2.0.CO;2.

——, and ——, 2004: The role of moisture in the dynamics and energetics of turbulent baroclinic eddies. *J. Atmos. Sci.*, **61**, 1693–1710, https://doi.org/10.1175/1520-0469(2004)061<1693:TROMIT>2.0.CO;2.

Lee, S., and I. M. Held, 1993: Baroclinic wave packets in models and observations. *J. Atmos. Sci.*, **50**, 1413–1428, https://doi.org/10.1175/1520-0469(1993)050<1413:BWPIMA>2.0.CO;2.

Lembo, V., F. Lunkeit, and V. Lucarini, 2019: TheDiaTo (v1.0) – A new diagnostic tool for water, energy and entropy budgets in climate models. *Geosci. Model Dev.*, **12**, 3805–3834, https://doi.org/10.5194/gmd-12-3805-2019.

Levine, X. J., and T. Schneider, 2015: Baroclinic eddies and the extent of the Hadley circulation: An idealized GCM study. *J. Atmos. Sci.*, **72**, 2744–2761, https://doi.org/10.1175/JAS-D-14-0152.1.

Li, L., A. P. Ingersoll, X. Jiang, D. Feldman, and Y. L. Yung, 2007: Lorenz energy cycle of the global atmosphere based on reanalysis datasets. *Geophys. Res. Lett.*, **34**, L16813, https://doi.org/10.1029/2007GL029985.

Lorenz, E. N., 1955: Available potential energy and the maintenance of the general circulation. *Tellus*, **7**, 157–167, https://doi.org/10.1111/j.2153-3490.1955.tb01148.x.

——, 1979: Numerical evaluation of moist available energy. *Tellus*, **31**, 230–235, https://doi.org/10.1111/j.2153-3490.1979.tb00901.x.

Lutsko, N. J., and M. Popp, 2018: The influence of meridional gradients in insolation and longwave optical depth on the climate of a gray radiation GCM. *J. Climate*, **31**, 7803–7822, https://doi.org/10.1175/JCLI-D-18-0103.1.

——, and M. C. Hell, 2021: Moisture and the persistence of annular modes. *J. Atmos. Sci.*, **78**, 3951–3964, https://doi.org/10.1175/JAS-D-21-0055.1.

——, I. M. Held, and P. Zurita-Gotor, 2015: Applying the fluctuation–dissipation theorem to a two-layer model of quasigeostrophic turbulence. *J. Atmos. Sci.*, **72**, 3161–3177, https://doi.org/10.1175/JAS-D-14-0356.1.

——, ——, ——, and A. K. O'Rourke, 2017: Lower-tropospheric eddy momentum fluxes in idealized models and reanalysis data. *J. Atmos. Sci.*, **74**, 3787–3797, https://doi.org/10.1175/JAS-D-17-0099.1.

——, J. W. Baldwin, and T. W. Cronin, 2019: The impact of large-scale orography on Northern Hemisphere winter synoptic temperature variability. *J. Climate*, **32**, 5799–5814, https://doi.org/10.1175/JCLI-D-19-0129.1.

Manabe, S., and R. T. Wetherald, 1975: The effects of doubling the CO_2 concentration on the climate of a general circulation model. *J. Atmos. Sci.*, **32**, 3–15, https://doi.org/10.1175/1520-0469(1975)032<0003:TEODTC>2.0.CO;2.

——, and ——, 1980: On the distribution of climate change resulting from an increase in CO_2 content of the atmosphere. *J. Atmos. Sci.*, **37**, 99–118, https://doi.org/10.1175/1520-0469(1980)037<0099:OTDOCC>2.0.CO;2.

Moore, R. W., and M. T. Montgomery, 2005: Analysis of an idealized, three-dimensional diabatic Rossby vortex: A coherent structure of the moist baroclinic atmosphere. *J. Atmos. Sci.*, **62**, 2703–2725, https://doi.org/10.1175/JAS3472.1.

O'Gorman, P. A., 2010: Understanding the varied response of the extratropical storm tracks to climate change. *Proc. Natl. Acad. Sci.*, **107**, 19 176–19 180, https://doi.org/10.1073/pnas.1011547107.

——, 2011: The effective static stability experienced by eddies in a moist atmosphere. *J. Atmos. Sci.*, **68**, 75–90, https://doi.org/10.1175/2010JAS3537.1.

——, and T. Schneider, 2008a: The hydrological cycle over a wide range of climates simulated with an idealized GCM. *J. Climate*, **21**, 3815–3832, https://doi.org/10.1175/2007JCLI2065.1.

——, and ——, 2008b: Energy of midlatitude transient eddies in idealized simulations of changed climates. *J. Climate*, **21**, 5797–5806, https://doi.org/10.1175/2008JCLI2099.1.

Panetta, R. L., 1993: Zonal jets in wide baroclinically unstable regions: Persistence and scale selection. *J. Atmos. Sci.*, **50**, 2073–2106, https://doi.org/10.1175/1520-0469(1993)050<2073:ZJIWBU>2.0.CO;2.

Pan, Y., L. Li, X. Jiang, G. Li, W. Zhang, X. Wang, and P. A. Ingersoll, 2017: Earth's changing global atmospheric energy cycle in response to climate change. *Nat. Commun.*, **8**, 14367, https://doi.org/10.1038/ncomms14367.

Pauluis, O., 2007: Sources and sinks of available potential energy in a moist atmosphere. *J. Atmos. Sci.*, **64**, 2627–2641, https://doi.org/10.1175/JAS3937.1.

——, 2011: Water vapor and mechanical work: A comparison of Carnot and steam cycles. *J. Atmos. Sci.*, **68**, 91–102, https://doi.org/10.1175/2010JAS3530.1.

——, and I. M. Held, 2002a: Entropy budget of an atmosphere in radiative–convective equilibrium. Part I: Maximum work and frictional dissipation. *J. Atmos. Sci.*, **59**, 125–139, https://doi.org/10.1175/1520-0469(2002)059<0125:EBOAAI>2.0.CO;2.

——, and ——, 2002b: Entropy budget of an atmosphere in radiative–convective equilibrium. Part II: Latent heat transport and moist processes. *J. Atmos. Sci.*, **59**, 140–149, https://doi.org/10.1175/1520-0469(2002)059<0140:EBOAAI>2.0.CO;2.

——, A. Czaja, and R. Korty, 2008: The global atmospheric circulation on moist isentropes. *Science*, **321**, 1075–1078, https://doi.org/10.1126/science.1159649.

Pavan, V., and I. M. Held, 1996: The diffusive approximation for eddy fluxes in baroclinically unstable jets. *J. Atmos. Sci.*, **53**, 1262–1272, https://doi.org/10.1175/1520-0469(1996)053<1262:TDAFEF>2.0.CO;2.

Pierrehumbert, R. T., H. Brogniez, and R. Roca, 2007: On the relative humidity of the atmosphere. *The Global Circulation of the Atmosphere*, T. Schneider and A. Sobel, Eds., Princeton University Press, 143–185.

——, D. S. Abbot, A. Voigt, and D. Koll, 2011: Climate of the neoproterozoic. *Ann. Rev. Earth Planet. Sci.*, **39**, 471–460, https://doi.org/10.1146/annurev-earth-040809-152447.

Raymond, D. J., 2013: Sources and sinks of entropy in the atmosphere. *J. Adv. Model. Earth Syst.*, **5**, 755–763, https://doi.org/10.1002/jame.20050.

Reed, R. J., M. D. Albright, A. J. Sammons, and P. Undén, 1988: The role of latent heat release in explosive cyclogenesis: Three examples based on ECMWF operational forecasts. *Wea. Forecasting*, **3**, 217–229, https://doi.org/10.1175/1520-0434(1988)003<0217:TROLHR>2.0.CO;2.

Romanski, J., and W. B. Rossow, 2013: Contributions of individual atmospheric diabatic heating processes to the generation of available potential energy. *J. Climate*, **26**, 4244–4263, https://doi.org/10.1175/JCLI-D-12-00457.1.

Romps, D. M., 2008: The dry-entropy budget of a moist atmosphere. *J. Atmos. Sci.*, **65**, 3779–3799, https://doi.org/10.1175/2008JAS2679.1.

Schneider, T., and C. C. Walker, 2006: Self-organization of atmospheric macroturbulence into critical states of weak nonlinear eddy–eddy interactions. *J. Atmos. Sci.*, **63**, 1569–1586, https://doi.org/10.1175/JAS3699.1.

——, and ——, 2008: Scaling laws and regime transitions of macroturbulence in dry atmospheres. *J. Atmos. Sci.*, **65**, 2153–2173, https://doi.org/10.1175/2007JAS2616.1.

——, and P. A. O'Gorman, 2008: Moist convection and the thermal stratification of the extratropical troposphere. *J. Atmos. Sci.*, **65**, 3571–3583, https://doi.org/10.1175/2008JAS2652.1.

——, ——, and X. J. Levine, 2010: Water vapor and the dynamics of climate changes. *Rev. Geophys.*, **48**, RG3001, https://doi.org/10.1029/2009RG000302.

Shaw, T. A., and R. J. Graham, 2020: Hydrological cycle changes explain weak snowball Earth storm track despite increased surface baroclinicity. *Geophys. Res. Lett.*, **47**, e2020GL089866, https://doi.org/10.1029/2020GL089866.

Sherwood, S. C., R. Roca, T. M. Weckwerth, and N. G. Andronova, 2010: Tropospheric water vapor, convection, and climate. *Rev. Geophys.*, **48**, RG2001, https://doi.org/10.1029/2009RG000301.

Singh, M. S., and M. E. O'Neill, 2022: The climate system and the second law of thermodynamics. *Rev. Mod. Phys.*, **94**, 015001, https://doi.org/10.1103/RevModPhys.94.015001.

Troen, I. B., and L. Mahrt, 1986: A simple model of the atmospheric boundary layer; sensitivity to surface evaporation. *Bound.-Layer Meteor.*, **37**, 129–148, https://doi.org/10.1007/BF00122760.

Wernli, H., S. Dirren, M. A. Liniger, and M. Zillig, 2002: Dynamical aspects of the life cycle of the winter storm 'Lothar' (24–26 December 1999). *Quart. J. Roy. Meteor. Soc.*, **128**, 405–429, https://doi.org/10.1256/003590002321042036.

Wills, R. C. J., and T. Schneider, 2018: Mechanisms setting the strength of orographic Rossby waves across a wide range of climates in a moist idealized GCM. *J. Climate*, **31**, 7679–7700, https://doi.org/10.1175/JCLI-D-17-0700.1.

Zhou, W., I. M. Held, and S. T. Garner, 2017: Tropical cyclones in rotating radiative–convective equilibrium with coupled SST. *J. Atmos. Sci.*, **74**, 879–892, https://doi.org/10.1175/JAS-D-16-0195.1.

Zurita-Gotor, P., 2005: Updraft/downdraft constraints for moist baroclinic modes and their implications for the short-wave cutoff and maximum growth rate. *J. Atmos. Sci.*, **62**, 4450–4458, https://doi.org/10.1175/JAS3630.1.

——, 2014: On the sensitivity of zonal-index persistence to friction. *J. Atmos. Sci.*, **71**, 3788–3800, https://doi.org/10.1175/JAS-D-14-0067.1.

——, J. Blanco-Fuentes, and E. P. Gerber, 2014: The impact of baroclinic eddy feedback on the persistence of jet variability in the two-layer model. *J. Atmos. Sci.*, **71**, 410–429, https://doi.org/10.1175/JAS-D-13-0102.1.